2005 ALCPG & ILC Workshops - Snowmass, U.S.A.

Instrumentation of the Very Forward Region of a Linear Collider Detector

W. Lohmann *
DESY, D-15738 Zeuthen, Germany

Calorimeters in the very forward region of the ILC detector are necessary to measure the luminosity delivered by the accelerator, to extend the coverage to small polar angles and to assist the beam tuning. A silicon-tungsten calorimeter, LumiCal, is planned to measure the luminosity. It will be placed at relatively large polar angles where background from beamstrahlung can be kept small. Calorimeters at smaller polar angles, denoted as BeamCal and PhotoCal, are hit by a large amount of beamstrahlung, hence radiation hard sensors are needed. BeamCal will extend the detector coverage for high energy electron detection down to about 5 mrad. BeamCal and PhotoCal will serve for tuning the beam to maximum luminosity. Monte Carlo simulations to optimize the design are performed. Technological options for the innermost calorimeters are discussed.

1. INTRODUCTION

The luminosity of a linear collider is determined using Bhabha scattering at small angles. Precision physics requires an accuracy of the luminosity measurement of better than $O(10^{-3})$ [1, 2]. For this purpose a special calorimeter, LumiCal, is planned. To ensure good hermeticity of the detector, a second calorimeter, BeamCal, is foreseen to cover very small polar angles just outside the beam-pipe. The latter is crucial for background suppression in new particle searches. The signature for many new particle channels is a few low energy particles in the detector and large missing energy and momentum. Two-photon processes may create a similar picture in the detector and have usually order of magnitudes larger cross sections. However, two-photon events can be identified if at least one of the high energy electrons is detected. Since at small polar angles large depositions from many low energy electrons and positrons from beamstrahlung appear, high energy electron detection is a challenge. The depositions from beamstrahlung depend on the beam parameters and will be measured in the BeamCal and PhotoCal, the latter positioned downstream, to assist in tuning the beams.

A possible layout of the very forward region of the ILC detector [3] is shown in Figure 1. The BeamCal adjacent to the beam-pipe covers a polar angle range between 4 and 28 mrad. The LumiCal is the luminometer of the detector and covers angles between 26 and 82 mrad. This layout is designed for head-on collisions or a small crossing angle. For 20 mrad crossing angle it must be reconsidered. In addition, a PhotoCal is considered at polar angles of 100 μrad to measure the tails of the beamstrahlung photons.

2. SIMULATION STUDIES

Simulations are done for all calorimeters to optimize their design for the functionality given above.

2.1. LumiCal Simulations

We simulate a silicon tungsten calorimeter. First the requirements on the tolerances of the inner radius of the calorimeter, of the distance between the two calorimeters on both sides of the interaction point, and of the displacement of the beam with respect to the nominal beam position are studied using the BHLUMI [4] program. As an

*On behalf of the FCAL Collaboration

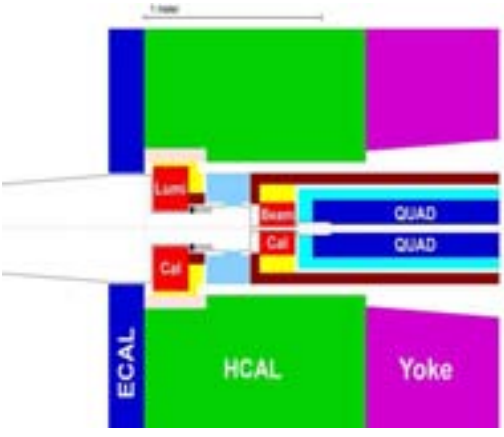

Figure 1: The forward calorimeters BeamCal and LumiCal. The conical beam-pipe on the left points to the interaction region. The distance between the interaction point (IP) and the LumiCal is about 3 m. ECAL and HCAL are the electromagnetic and hadron calorimeters, respectively, and QUAD is the last quadrupole of the beam delivery system.

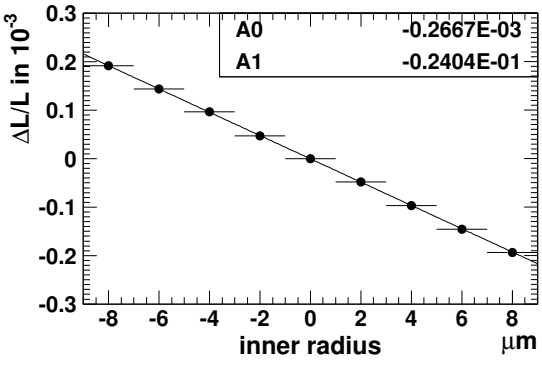

Figure 2: Relative variation of the cross section of Bhabha scattering in the polar angle range of LumiCal as a function of a shift in the inner calorimeter radius.

example, in Figure 2 is shown the variation of the detected Bhabha cross section as a function of a shift of the inner calorimeter radius. To maintain the accuracy of about 10^{-4}, the inner acceptance radius must be controlled with an accuracy of a few μm. In a similar way, the allowed uncertainties on the other two quantities are estimated. The distance between the two calorimeters and the radial beam position must be controlled with precisions of 60 μm and 200μm, respectively [5].

A full shower simulation and reconstruction is done using the BRAHMS [6] package which is based on the Geant 3.21 [7] detector simulation program. Bhabha scattering events are generated with the BHLUMI and BHWIDE [8] packages. The program CIRCE [9] is used to include beamstrahlung losses. Two versions of a silicon-tungsten calorimeter are simulated. In the first version (pad), the silicon sensor planes are subdivided radially into rings and azimuthally into sectors, forming readout pads. Longitudinally the calorimeter is composed of layers, each layer consisting of a tungsten absorber disk and a sensor plane. The energy deposited on each pad is read out. The thickness of the tungsten layer is one radiation length and the gap for sensors is chosen to be 3 mm. The sensor thickness is 0.5 mm. In the basic pad design each sensor plane is subdivided into 15 rings and 24 sectors. In the second version (strip), the absorber structure is similar. The sensor planes alternate between sensors with 64 concentric strips and sensors with 120 radial sectors. In depth, both calorimeters are composed of 30 layers.

The position of the showers in both versions is reconstructed from the energy depositions on the sensors pads or strips using a weight function W_i:

$$< x >= \frac{\sum_i x_i W_i}{\sum_i W_i}. \tag{1}$$

Only significant depositions are considered, introducing the following logarithmic weight function [10]:

$$W_i = \max\{0, [C + \ln \frac{E_i}{E_{Total}}]\}. \tag{2}$$

The constant C is determined by an optimization process under two criteria: best resolution and minimum bias in the polar angle θ. Using the weight of eqn. 2, the resolution in θ, σ_θ, is improved, in comparison to a simple 'center of gravity' weighting, by a factor of about three.

The resolution σ_θ is shown as a function of C in Figure 3 for a beam energy of 250 GeV. For a value of C=6.8 the best resolution in θ, σ_θ=1.3 $\times 10^{-4}$ rad, is obtained. For the same value the bias in θ is 10^{-5} rad [11].

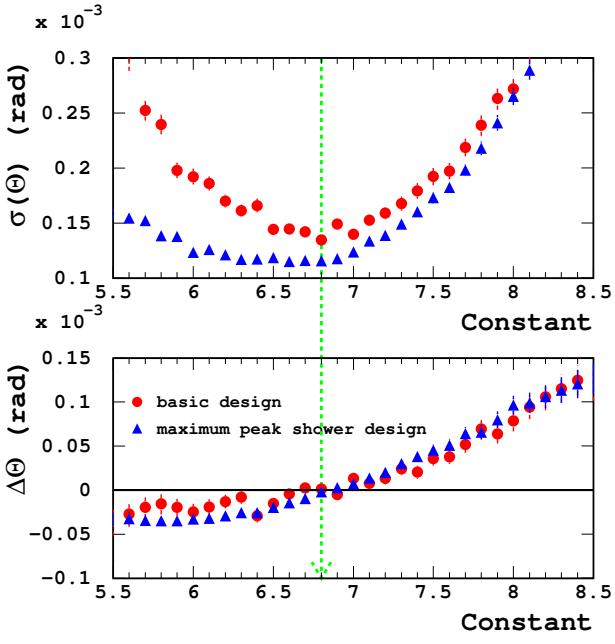

Figure 3: The resolution in the polar angle θ, $\sigma(\theta)$ (top), as a function of the constant C used in the logarithmic weighting for a beam of 250 GeV. The shift, $\Delta\theta$ (bottom), between the generated and reconstructed polar angle. The dots and triangles are the results for the 'basic' and 'maximum peak shower' design, respectively.

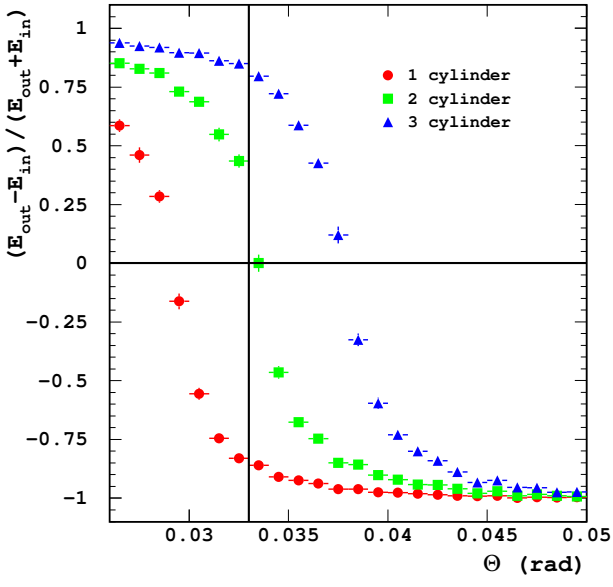

Figure 4: The normalised difference of energies deposited on the rings defining the inner acceptance region. The results correspond to one (dots), two (squares) and three (triangles) sensor pad rings being outside the acceptance region and defining the minimum acceptance angle θ_{min}.

The resolution in θ can be improved by a finer segmentation of the sensor planes in the range of the shower maximum and a coarser segmentation at the front and rear end of the calorimeter, the 'shower peak' design, as shown in Figure 3. The best value for the resolution is σ_θ=1.1 $\times 10^{-4}$ rad at C=6.8. The bias is compatible with zero. The simulation of the 'strip' version gives similar results for σ_θ.

The energy resolution is obtained from a Gaussian fit of the reconstructed shower energy distribution. It can be parametrized as in $\Delta E/E = 0.25/\sqrt{E}$ for the pad version and $\Delta E/E = 0.31/\sqrt{E}$ for the strip version of the calorimeter, where the energy is given in GeV.

The quantity finally needed for the luminosity calculation is the number of Bhabha events in a certain polar angle range. Due to the steep fall off of the Bhabha cross section as a function of θ, the definition of the inner radius of the acceptance region is critical for the luminosity accuracy. One possibility is to apply the acceptance cut on the measured θ angle of the reconstructed shower position. In that case all sensor layers must be precisely aligned and the bias in θ must be controlled. A second possibility is to use the energy deposited onto a few precision sensor layers in the center of the shower. The sharing of the deposited energy between two precision rings of pads is used to decide whether an event is inside or outside the acceptance region. Applying loose selection cuts on the energy balance and acollinearity of the event, the distribution of the cut quantity using three precision layers is shown in Figure 4. Due to the sharp step-function behavior this method seems to be very promising for the definition of the acceptance region.

The studies done so far are valid for zero or 2 mrad crossing angle. For a crossing angle of 20 mrad beamstrahlung remnants are spread into the current angular coverage of the LumiCal. A new design of the forward region must be worked out.

2.2. BeamCal Simulations

The BeamCal will be hit by the electrons and positrons originating from beamstrahlung photon conversion. As an example, a simulation of the energy density per bunch crossing at the front face of the BeamCal as a function of the distance from the beam axis and the azimuthal angle ϕ is shown in Figure 5 for a center-of-mass energy of 500 GeV. The distribution is obtained using the Monte Carlo program GuineaPig [12]. The energy density drops rapidly with growing radius. In addition, a ϕ dependence due to the flat beam and the action of the solenoidal field inside the detector, is observed. The maximum energy density occurs near the top and bottom regions. The total deposited energy amounts to about 30 TeV per bunch crossing for zero or 2 mrad crossing angle. For a crossing angle of 20 mrad the depositions are about a factor of 3 larger and, depending on the magnetic field configuration, spread out over a larger area.

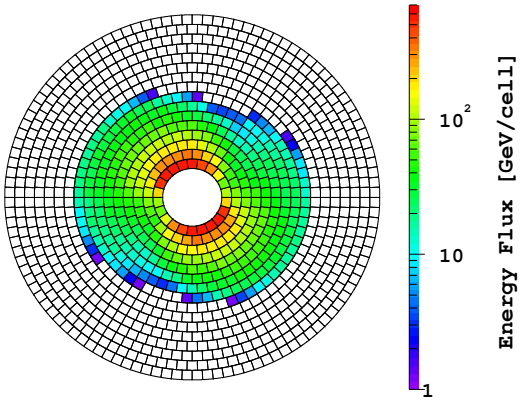

Figure 5: Energy density of beamstrahlung remnants per bunch crossing in the R-ϕ plane at the face of the BeamCal. The centre-of-mass energy is 500 GeV and TESLA machine parameter settings are used.

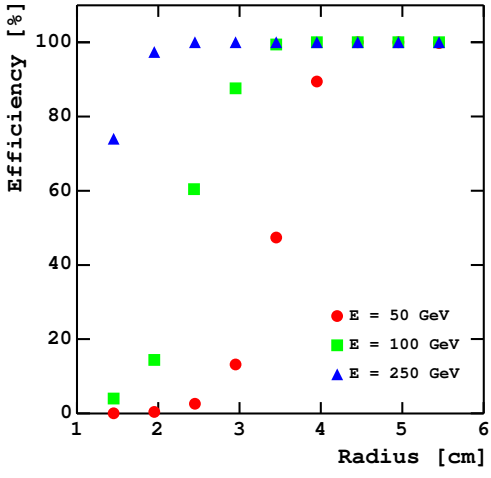

Figure 6: The efficiency to detect an electron of energy 50, 100, 250 GeV as a function of the radius in the region with high background in the sampling calorimeter.

The reconstruction efficiency of single electrons is studied for a diamond-tungsten sandwich calorimeter and a crystal calorimeter made of $PbWO_4$. The simulations are done for 500 GeV centre-of-mass energy for TESLA standard beam parameters [13]. Beamstrahlung is generated using GuineaPig [12]. About 12000 electrons and positrons with an average energy of 1.7 GeV hit each side of BeamCal. Isolated high energy electrons are simulated with energies between 50 and 250 GeV. The response of the calorimeters is simulated using the GEANT3 [7] based detector simulation program BRAHMS [6]. The simulated sampling calorimeter is longitudinally divided into 30 disks of tungsten, each 1 X_0 thick, interleaved by diamond active layers of 0.5 mm. The Molière radius is about 1 cm. The sensitive planes are divided into pads with a size of about half a Molière radius in both dimensions, as shown in Figure 5. This pad size was found to give the best performance [14]. Bunch crossings are simulated with and without a single high energy electrons. The energy in each cell is read out, and an algorithm [3] is applied to reconstruct the single high energy electrons. The algorithm is also applied to pure beamstrahlung events to determine the electron fake rate.

The efficiency to detect electrons is shown in Figure 6, for several electron energies, for regions in the sandwich calorimeter with relatively high background ($\phi \approx 90°$). An electron of 250 GeV is detected with almost 100% efficiency. The efficiency drops near the innermost radius, partly due to shower leakage. Electrons of 50 GeV are identified with high efficiency only at larger radii. Similar investigations are done with a heavy element crystal calorimeter. The segmentation in the R-ϕ plane is again about half a Molière radius. Three pieces in depth are used, as shown in Figure 7. The segmentation in depth is 3 X_0 for the front piece, 9 X_0 for the middle and 8 X_0 for the rear piece, where X_0 is the radiation length. This segmentation is optimized to minimize the electron fake

rate. The efficiency to detect a 100 GeV electron as a function of the radius is shown in Figure 8 and compared with the result from the sampling calorimeter. The performance of the sampling calorimeter is superior. Monte Carlo simulations have shown that a finer segmentation of the crystal calorimeter will not improve the performance. Because a larger number of fibers will reduce the volume filled with the heavy element crystals, the transverse shower shape is distorted and energy leaks from the front to the rear side.

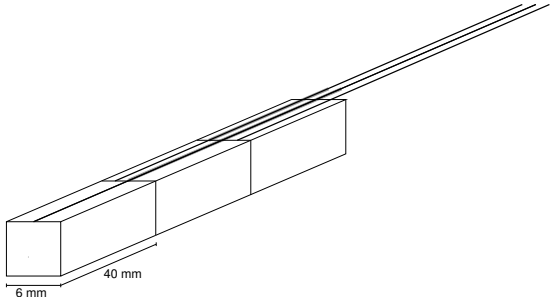

Figure 7: Scintillator pieces forming a segment of the crystal calorimeter. Each piece is connected to an optical fiber of 1 mm diameter which is optically isolated from the other pieces adjacent to the rear end of the calorimeter.

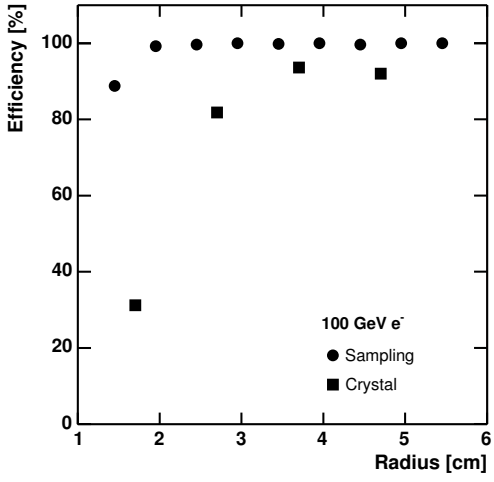

Figure 8: The efficiency to detect a 100 GeV electron as a function of the radius in the low background region for a crystal (squares) and sampling (dots) calorimeter.

The studies for the sandwich calorimeter reported above are done on the basis of the QED processes included in the Monte Carlo package GuineaPig [12] for an ideal accelerator (ideal beam simulation). They are repeated for a more realistic beam simulation, including the simulation of beam transport through the linac and the beam delivery system, wake-field and ground motion effects, the behavior of the beam-feedback system and a luminosity optimization at the beginning of the bunch-train crossing [15]. The total energy deposited in the BeamCal is up to 30% larger for the realistic beam simulation. However, the rms of the energy depositions in a certain pad from a sequence of bunch crossings is similar to the ideal case. The detection efficiency using realistic beam simulation is only a few % less at small radii. The fake electron rate of about 1% for realistic beam simulation is at the same level as for ideal beam.

Similar studies done for a beam crossing angle of 20 mrad show comparable results [16].

2.3. Beam Diagnostics

The spatial and spectral distributions of the beamstrahlung photons and the electrons and positrons from pair productions depend on the beam parameters. The photons follow within a cone of a few hundred μrad the beam direction and can be detected with a calorimeter about 100 m downstream. To measure the tails of their angular distribution, a calorimeter similar to the diamond-tungsten sandwich calorimeter is used replacing the diamond sensors by a heavy gas, e.g. C_3F_8. The shower particles ionize the gas and the electrons from the ionization are collected by copper pads on a printed circuit board. The boards are positioned in the center of the gap between two tungsten absorber disks. The calorimeter covers polar angles between 100 μrad and 400 μrad. Azimuthally the calorimeter is subdivided into four sectors and the total deposition in each sector is measured. From the energy deposited in each sector and from left-right and top-bottom asymmetries, beam parameters are derived bunch-by-bunch using a neural network. The accuracies obtained are given in Table I.

Similar studies are done using the energy distribution of electron and positron pairs in the BeamCal [17]. Appropriately defined moments of the energy distribution allow to determine beam parameter bunch-by-bunch. The

Table I: The accuracies reached for several beam parameters from the analysis of the energy depositions in the Photocal

Quantity	nominal value	precision
bunch width in x	553 nm	4.2 nm
bunch width in y	5.0 nm	0.1 nm
bunch length in z	300μm	7.5μm
beam offset in x	0	4 nm
beam offset in y	0	0.16 nm

precision reached is very similar to the one obtained from PhotoCal, however, here additional measurements are available, and there is hope to improve in the determination of several beam parameters simultaneously using both devices. Also studies for a crossing angle of 20 mrad are promising.

3. FORWARD CALORIMETER R&D

Research is done on the mechanical frame of LumiCal, on a position and alignment monitor and on sensors.

3.1. Mechanics and Alignment of LumiCal

A possible mechanical design in shown in Figure 9. The calorimeter consists of two half barrels to allow for

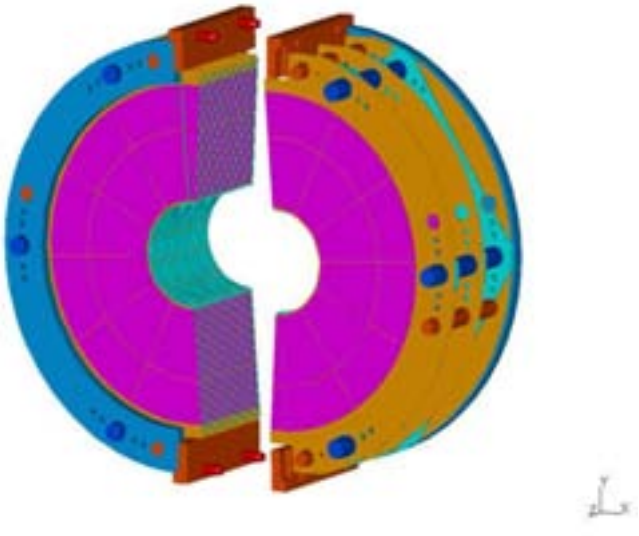

Figure 9: The mechanical structure of the LumiCal. The thicker bolts support the tungsten disks. The red bolts form a precision frame to position the sensor layers. Holes in the support ring are foreseen to allow a precise optical survey after the calorimeter is mounted.

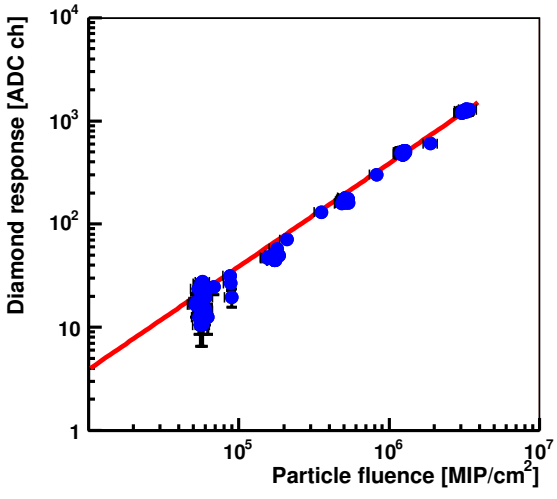

Figure 10: The response of a diamond sensor as a function of the particle flux per cm^2 and 10 ns.

mounting on a closed beam pipe. The heavy part, the tungsten half disks, are supported by the thicker bolts. The accuracy requirements for this frame are moderate.

The thinner bolts carry only the sensor half layers. This frame is decoupled from the tungsten disk support, hence it does not suffer by gravitational sag due to the heavy tungsten disks. The silicon sensors of 300 μm thickness are

glued on a 1 mm thick ceramic support. Space is left for bonding. The frame of the thinner bolts has to fulfill the extreme precision requirements for the sensor positioning. In order to be able to survey the precision layers in the center of the device after mounting, the support ring contains holes.

The luminosity measurement requires precise alignment of the two LumiCal detectors to each other and precise positioning with respect to the beam-line and the interaction point. The position monitoring should not interfere with the mechanical support of the detector, hence an optical system is preferred. We plan a laser system with a CCD matrix sensor to measure the displacement of the LumiCal detector with respect to the beam pipe flange. A fine pixel CCD matrix offers X-Y measurements in a single position detector. The pixel size can be 5 μm $\times$ 5 μm on the 7 mm$\times$ 7 mm matrix. The laser beam spot will have the diameter of about 100-300 μm. A study was made using a CCD matrix with 640x480 pixels of 20 x 20 μm^2 size. An accuracy of about 1 μm for the monitoring of the displacement of a reference frame was reached [18].

3.2. Sensor Studies

Diamond sensors of 1 cm^2 area were obtained from several manufacturers and electrical properties, the response for ionizing particles and the behavior under low (up to 100 Gy) radiation doses are investigated. The results are promising, however the homogeneity of the response from sensors of different raw wafers is still a problem. Linearity studies using the fast extraction mode of the CERN PS beam are ongoing [19]. A preliminary result is shown in Figure 10. Linearity within 30% was observed over a flux range between 1 and 10^6 particles per cm^2 and 10 ns. However, the flux calibration is understood only with the same level of accuracy.

Scintillator segments, as shown in Figure 7, are studied with cosmic muons. Reading out the scintillator piece via the fiber reduces the number of photoelectrons to about 15%, sufficient for the application in a calorimeter. Also the response of a non-scintillating heavy element crystal was studied. The wavelength-shifting fiber converts the Cerenkov light with a reduction of the number of photoelectrons similar to the case of a scintillator [19].

A heavy gas ionization chamber, as foreseen for the PhotoCal, was tested successfully in the PS beam at Protvino [20]. The chamber was filled with C_3F_8 and signals were collected from 4x4 cm^2 pads. Good linearity is observed in the energy range considered. Further tests are planned with smaller pad sizes and to study the linearity over a wider dynamic range.

3.3. Acknowledgments

The author would like to thank all members of the FCAL collaboration. Only the joint effort made the presentation of these results possible.

References

[1] TESLA Technical Design Report, DESY 2001-011, ECFA 2001-209, March 2001.

[2] K. Moenig, talk at the Workshop "'Instrumentation of the Forward Region of a Linear Collider Detector"', 26-27 August 2004, DESY-Zeuthen, Germany, http://www-zeuthen.desy.de/lcdet/.

[3] H. Abramowicz et al., IEEE Trans. Nucl. Sci. **51**, 2983 (2004).

[4] S. Jadach *et al.*, Comp. Phys. Comm. **102**, 229 (1997).

[5] A. Stahl, *Luminosity Measurement via Bhabha Scattering: Precision Requirements for the Luminosity Calorimeter*,

[6] T. Behnke et al., *BRAHMS: A Monte Carlo for a Detector at a 500/800* GeV *Linear Collider.* LC-TOOL-2001-005, (2001).

[7] R. Brun, *et al.*, *GEANT3*, Preprint CERN DD/EE/84-1, 1984, revised September 1987.

[8] W. Placzek et al., Phys. Lett. **B390**, 298 (1997).
[9] T. Ohl, hep-ph/9607454-rev.
[10] T.C. Awes *et al.*, Nucl. Instrum. and Methods, vol. **A 311** (1977).
[11] H. Abramowicz , *Luminosity measurement*, these proceedings.
[12] D. Schulte, *Study of Electromagnetic and Hadronic Background in the Interaction Region of the TESLA Collider*, Thesis, Hamburg University 1996, http://www-sldnt.slac.stanford.edu/nlc/beamdeliveryhome.htm.
[13] ILC-TRC Second Report, http://lcdev.kek.jp/TRCII/REPORT.HTM.
[14] A. Elagin, *The Optimized Sensor Segmentation for the Very Forward Calorimeter*, these proceedings. LC-DET-2005-004.
[15] D. Schulte *et al.*, *Intra-Bunch-Train Luminosity Optimisation for the TESLA Linear Collider* DESY-M-03-01R, Proceedings of the 2003 Particle Accelerator Conference, Portland, Oregon, 2736 (2003).
[16] T. Maruyama, *Pair Backgrounds and Electron ID for a 2-photon Veto*, Victoria Linear Collider Workshop, 2004; http://www.linearcollider.ca:8080/lc/vic04/abstracts/detector/ipbi/agenda.
[17] A. Stahl, *Diagnostics of Colliding Bunches from Pair Production and Beam Strahlung at the IP*, LC-DET-2005-003; H. Yamamoto, *Beam Profile Monitor*, MDI workshop, SLAC 2005, http://www-conf.slac.stanford.edu/mdi/sessions.htm.
[18] W. Wierba, J.Zachorowski and K. Oliwa, Report No 1931/PH, www.ifj.edu.pl/reports/2003html, Institute of Nuclear Physics, Cracow (2003).
[19] E. Kousnetzova, *Calorimeter technologies for forward region instrumentation*, proccedings of the LCWS, Stanford, March 2005.
[20] V. Bezzubov *et al.*, Nucl. Instrum. and Methods, vol. **A 494**, 369 (2002).